An experimental setup for investigating the blowdown of liquid CO2 down to -50°C

Didier Jamois, Christophe Proust, Leyla Teberikler, Adil Fahmi

An experimental setup for investigating the blowdown of liquid CO_2 down to -50°C

Didier Jamois [a], Christophe Proust [a,b], Leyla Teberikler [c], Adil Fahmi [d]

[a] *Ineris, Parc Technologique Alata, BP2, 60550 Verneuil-en-Halatte, France*
[b] *Sorbonne University, TIMR Laboratory, UTC-ESCOM, 60200 Compiègne, France*
[c] *TotalEnergies, EP Norge AS, Finnestadveien 44, 4029 Stavanger, Norway*
[d] *Equinor, Arkitekt Ebbells veg 10, 7053 Trondheim, Norway*

ABSTRACT

In many Carbon Capture and Storage (CCS) technologies, CO_2 is transported in a dense phase between 1 and 10 MPa, depending on the temperature. Previous investigations demonstrated that major accidents may occur during transportation or transfer operations in case of vessel or pipe depressurization to the atmosphere. Among the scenarios potentially leading to this, tank blowdown is a major concern due to two factors: the risk of brittle rupturing caused by low temperatures and the possibility of dry ice formation in the piping. Current flow models cannot properly model this, and further experimental evidence and detailed data are required.

To provide the required information, a specific experimental setup was developed and tested. The tank is a 2 m^3 sphere, carefully insulated and connected to a 40 mm diameter, 3 m long release pipe terminated by a discharge orifice to control the depressurization rate. The pipe can be connected either on the side of the vessel to release the gaseous phase or at the bottom to release the liquid phase.

Optic ports are provided on the vessel and on the pipe to observe phase transition and monitor the liquid level. The instrumentation is a set of pressure transducers and arrays of thermocouples inside the CO_2 and in the shell of the vessel. The tank is continuously weighed during the blowdown and the data are treated so that the mass flowrate can be obtained.

The performance of the system is discussed based on a gaseous phase blowdown starting from a half-filled vessel with liquid CO_2 at -38°C and 1 MPa. Detailed data are presented and discussed. All phases - liquid, gas, and solid - appeared during the release, and temperatures dropped to nearly -80°C in the shell and lasted for hours.

Keywords: Carbon Capture Storage, CO_2 vessel, Depressurization, Mass Flowrate, Dry Ice, Triple point state, Heat Exchange Rate

Nomenclature

Cp *specific heat capacity, J/(kg.K)*
e *thickness, mm*

m *mass, kg*
h *heat exchange rate, W/m²*
L_l *liquid level, m*
$\dot{Q}$ *thermal loss, W*
R *radius, mm*
T *temperature, ° C*
t *time, s*
VF *volume fraction*
V *volume, m³*
λ *thermal conductivity, W/(m.K)*
Φ *thermal flux, W*

Indexes
bo *bottom part*
fl *fluid*
fo *foam*
g *gas phase*
l *liquid phase*
st *steel*
up *upper part*
v *vessel*

1. INTRODUCTION

The Carbon Capture and Storage (CCS) concept is entering into a demonstration phase at the industrial level (European Zero Emission Technology and Innovation Platform, 2021) requiring the testing of process equipment (vessels, pipes, valves, flowmeters, compressors, …) and exploitation procedures of the networks. In CCS processes, CO_2 can be stored and transported in a dense phase at ambient temperature (10 to 45 °C) and at a pressure between 7 and 15 MPa (Peletiri et al., 2018). Alternatively, typically in maritime vessels, CO_2 can be stored at a reduced pressure of about 1 MPa but at a lower temperature of -40°C.

In CCS, safety is identified as an issue since extended toxic clouds may result from a catastrophic rupture of a containment (CO2Piphaz, 2009; Talemia et al., 2016; Woolley et al., 2014). A potentially hazardous situation is the fast blowdown of a vessel containing dense CO_2. This could be an accident situation but may also be intentional, typically in emergency situations. Since CO_2 can be regarded as a refrigerant with a strong cooling capability, a very large temperature drop can be expected which might favour vessel/pipe rupturing either due to thermal stress or to a transition from the ductile to the brittle material behaviour regime. In addition, dry ice might appear that could plug the pipes, not only stopping the operations but also putting the piping at risk.

A good understanding of the heat transfer and thermodynamic phenomena occurring during the blowdown is required to size the CCS equipment. Unfortunately, modelling the complete blowdown processes, which incorporates the

coexisting solid/liquid/gaseous phases, transients and heat transfer to the walls, remains very difficult (Haque et al., 1992a, 1992b; Martynov et al., 2018) and experimental data covering all those aspects are required. In particular, available experimental data of CO_2 vessel blowdown, especially at a large scale, is scarce (Jamois et al., 2015). Experimental results compatible with the industrial scale are thus required and need to be sufficiently detailed to allow the development of models. The objective of the present work is to develop and test an experimental method to produce the expected experimental data.

In the following, a new experimental setup is presented aiming at measuring the most important heat transfer and thermodynamic parameters during the blowdown of a large vessel (2 m^3) containing liquid CO_2 (initial pressures between 1 and 10 MPa, initial temperature between -50°C and 20°C). The temperatures inside the wall of the vessel, in the vapor phase and in the liquid phase are measured. The pressure is also recorded as well as the evolution of the total quantity of CO_2 remaining in the vessel from which the instantaneous mass flowrate is derived. The liquid level can also be monitored using a video recording of the interior of the vessel.

The hardware is described in the first section and the measurement techniques in the second one. In the third section, a typical blowdown test (pure CO_2, -38°C, 1 MPa) is presented and discussed.

2. EXPERIMENTAL SYSTEM

Choosing the dimensions of an experimental facility that can simulate industrial configurations and enable accurate monitoring of parameters, all at a “reasonable” cost, is always a challenge. To meet this constraint, a device as small as possible is preferred. However, to be able to scale up to the industrial scale, the dimensions of the setup should still be large enough.

The typical volume of high-pressure tanks is 10 m^3, while low-temperature storage tanks can have a volume of several tens of m^3. The wall thickness of these tanks is at least 5 cm. Pipe diameters are of the order of several inches. The most important parameters are heat exchange coefficients which depend on the exchange regime (turbulent, laminar) and linear scales such as the diameter of the vessel/pipe or thickness of the wall. Regarding heat transfer in the vessel, the characteristic dimension of the experimental tank should not be smaller than 1 m and the thickness of the wall should be a few centimetres. By experience, the pipe diameter should not be smaller than 2 inches (50 mm) otherwise the heat transfer and momentum exchange differ from what happens at the real scale.

2.1 THE VESSEL

The vessel presented in Figure 1 is a 2 m^3 steel sphere (actually 2.030 +/- 0.005 m^3, evaluated geometrically) consisting of two hemispherical shells welded together. This equipment was previously used to blow down various fluids (Chaineaux, 1993; Chaineaux,1995; Witlox et al., 2009; Lacome et al., 2020; France Nord, 2012; Woolley et al., 2013; Jamois et al., 2013; Gant et al., 2014; Zheng et al., 2017) but was significantly modified and upgraded to perform the present study.

The characteristics of the steel are given in Table 1. The inner radius is 778 mm and the mean wall thickness is 54 mm (+/-5 mm). The vessel is designed to withstand a static internal (service) pressure of 20 MPa. Electrical heating cables are attached to the external wall, allowing it to be heated up to 200 °C. The vessel is equipped with three flanges to introduce the measurement wiring, to feed the CO_2, and to blow down the vessel. The total weight of the vessel is 4.80 tonnes.

TABLE 1 - MAIN CHARACTERISTICS OF 2M^3 VESSEL STEEL*

STEEL GRADE	P355GH (1.0473)
TENSILE STRENGTH	>335 MPa
YIELD STRENGTH	≈ 600 MPa
λ_{ST}, **THERMAL CONDUCTIVITY** at ambient temperature*	44 W/mK
C_{PV}, **HEAT CAPACITY** at ambient temperature*	450 J/kg.K
ρ_V, **DENSITY***	7800 kg/m3

*: from Bjelic et al (2016) for P355GH steel

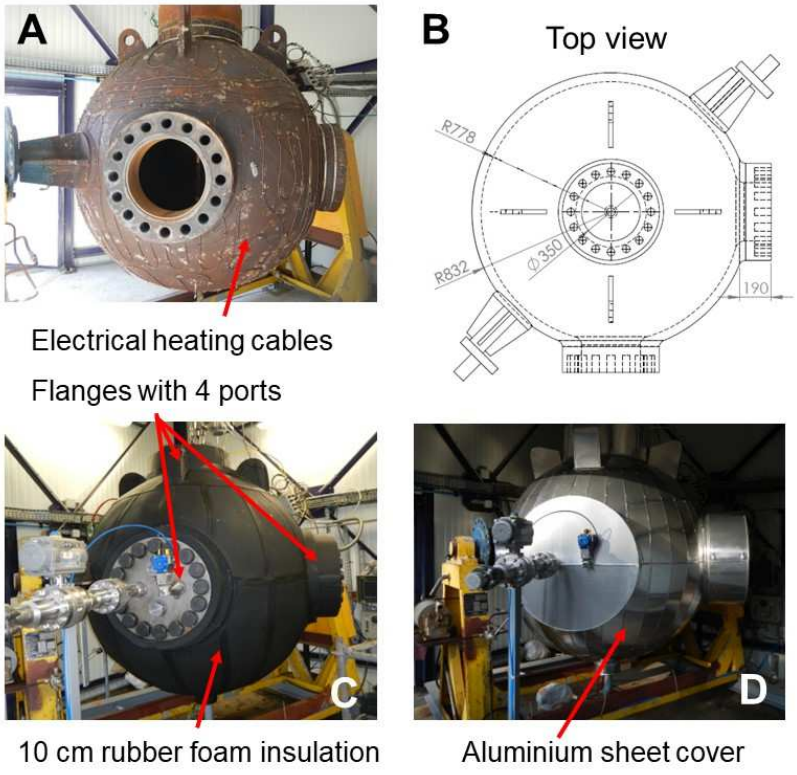

Figure 1: The 2m^3 steel vessel. (A) bare, (B) Top view drawing, (C) with the flanges and the insulation, (D) with aluminium sheet cover

To run cryogenic tests, it was compulsory to insulate the vessel. Note that for any initial test conditions, even outside the cryogenic domain, minimizing heat

exchanges with the surrounding provides a sort of worst-case situation in terms of temperature drop in the vessel wall.

Only a few insulation materials are suitable for low temperatures. Rubber foam was chosen and glued on the external wall of the vessel as shown in Figure 1. A verification of the quality of this insulation method was performed.

The foam thickness is 10 cm, and the rubber foam thermal conductivity is λ_{fo}= 0.034 W/m.K. The outer vessel surface area is 11 m^2, so that the global heat exchange coefficient should be about h= 3.75 W/K.

To verify this, the vessel was heated up to 31°C using the electrical heating cables. The temperature of the shell was monitored using the thermocouples inserted in the wall (this arrangement is described in the next section). After stopping the heaters, the temperature decrease is monitored as a function of time as shown in Figure 2. The average power $\dot{Q}_v$ dissipated during a time slot Δt is obtained from the first principle as:

$$\dot{Q_v} = {}^{m_v . C_{p_v} . \Delta T}/_{\Delta t} \qquad [1]$$

Where ΔT is the temperature drop during Δt. The slope is nearly linear. A temperature drop of ΔT = 8 °C occurs in a duration of Δt = 45 h (the average outside temperature stayed almost steady during this period at 2 °C +/-1 °C) giving an average power loss of 107 W. Since the mean temperature gap between the inside and the outside of the vessel is 25 °C, the measured heat exchange coefficient is h=4.3 W/K. This is somewhat larger than the theoretical value possibly because of the existence of thermal bridges (ports, supports,..) not accounted for in the theoretical estimation.

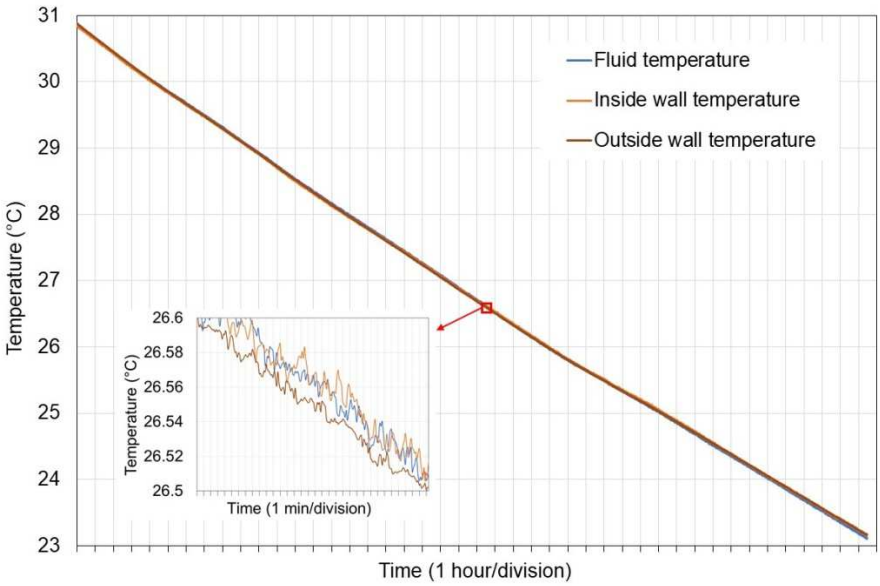

Figure 2: Temperature curves recorded during the cooling of the insulated vessel from 31°C to ambient (outside temperature = 2°C)

Finally, two CO_2-resistant optic ports (glass) were installed to see inside, detect phase changes and estimate the liquid level (explained in § 4.3). One is used to introduce light and the other for the video camera. These optic ports may be screwed in any threaded holes drilled in the three flanges of the vessel (Figure 3).

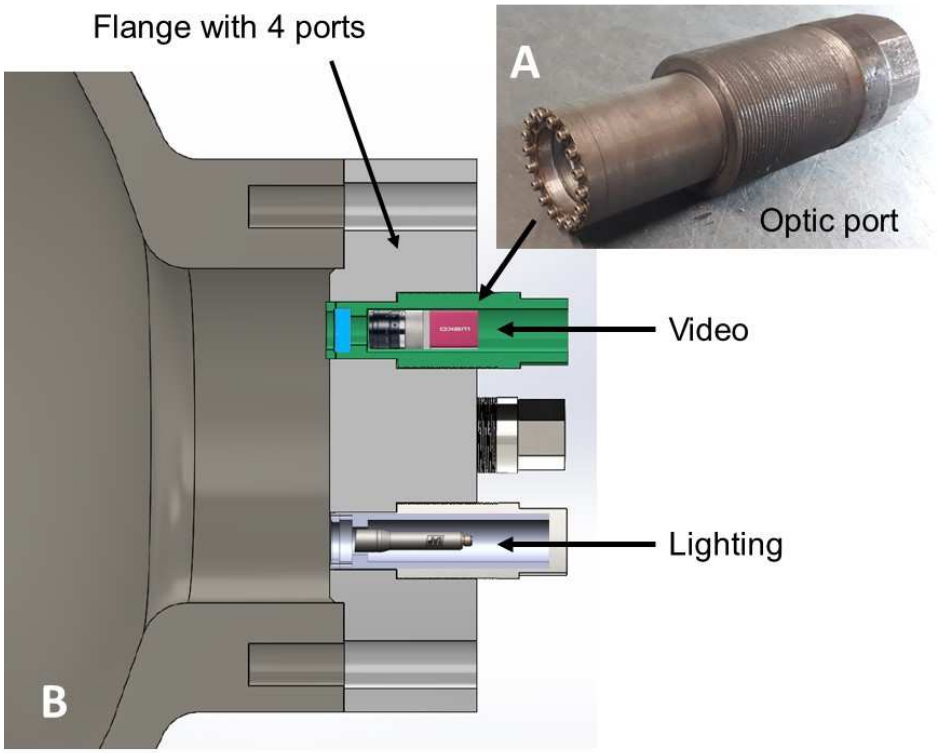

Figure 3: Optic port setup. (A) picture of an optic port, (B) drawing of the cross-section of a flange with two optic ports screwed inside and with a camera located inside one port and a lighting device inside a nearby one

2.2 THE PIPE

A 2 m long pipe, 40 mm inner diameter, equipped with a calibrated orifice (4 mm in the situation described in the “results” section § 4) is used to blow down the vessel. It can either be connected to the side flange for a purely gaseous phase release or at the bottom for a liquid phase release.

To observe any phase changes a transparent section was prepared (Figure 4). To avoid optical deformations, the transparent walls should be flat, meaning a square cross-section. Since the rest of the pipe has a circular cross-section a transitional section of pipe (circular to square) was built to limit the disturbance of the flow perturbation. The first criterion is that the cross-section (and thus flow velocity) should be kept constant all along the pipe whatever the shape of the cross-section. Nevertheless, the flow lines are disturbed, especially close to the wall. To avoid shear layer detachment phenomena, the second criterion is that any flow divergence angle should remain smaller that the critical shear layer detachment angle (10°). To achieve this, the length of the transitional section is 10 times that of the pipe diameter. Despite those precautions, the hydraulic diameter is different between the square and the circular cross section, but the gap is only 10% which is believed to be small enough.

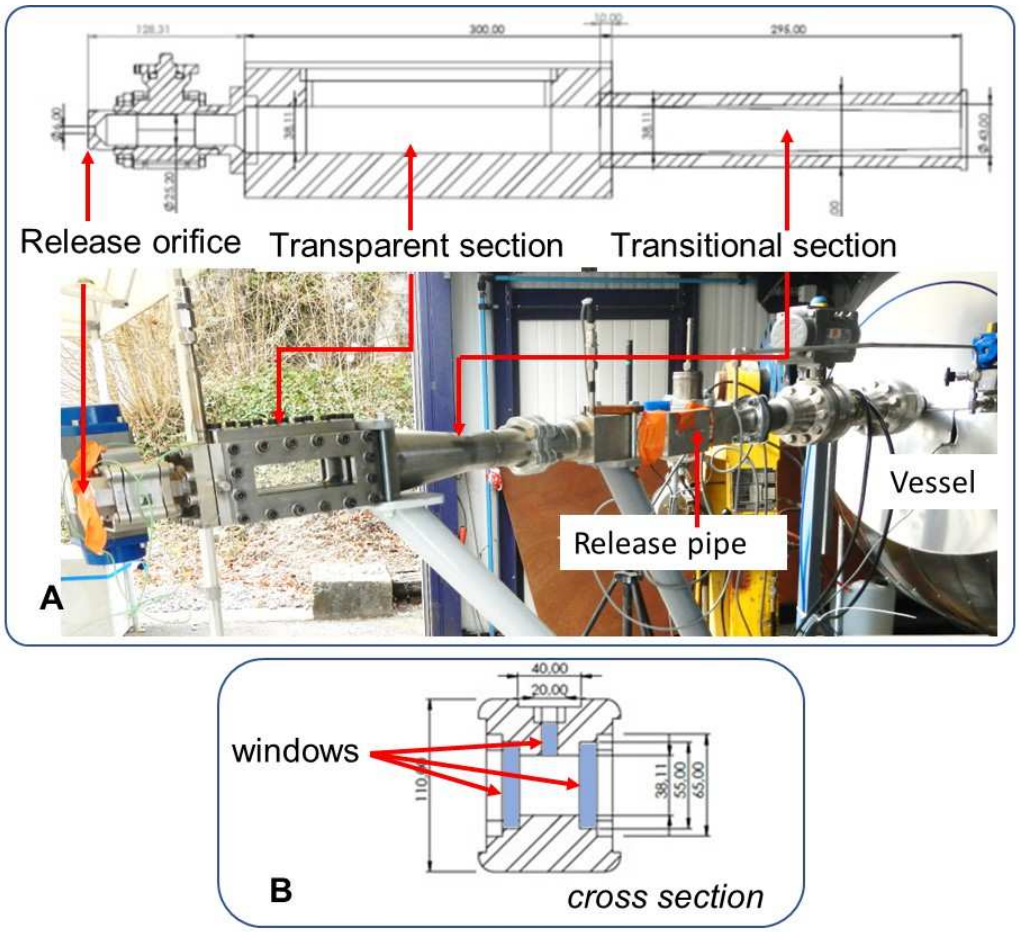

Figure 4: Transparent section. (A) Schematic and picture of the transparent section with the transitional section connected to the release pipe and to the vessel, (B) cross-section with the 3 windows

The transparent section is equipped with three windows. The camera is installed in front of one of the large windows while the parallel window is used to control the background light and to improve the contrast and resolution (like in Schlieren techniques). The top smaller window (Figure 4 B) is used to introduce a laser sheet to apply a particle image velocimetry (PIV) based technique.

The extremity of each pipe is equipped with the release valve installed immediately upstream from the release orifice (Figure 4 A). The distance between the orifice plate and the entrance of the valve is about 100 mm. The time to the full opening of this valve is about 1 s. Different release diameters may be used (from 1 mm to full bore).

The pipe is isolated from the vessel during the filling of the vessel. To avoid the production of a strong shock wave when opening the isolation valve, the pressures on both sides of this valve are first equalized using a bypass as shown in Figure 5.

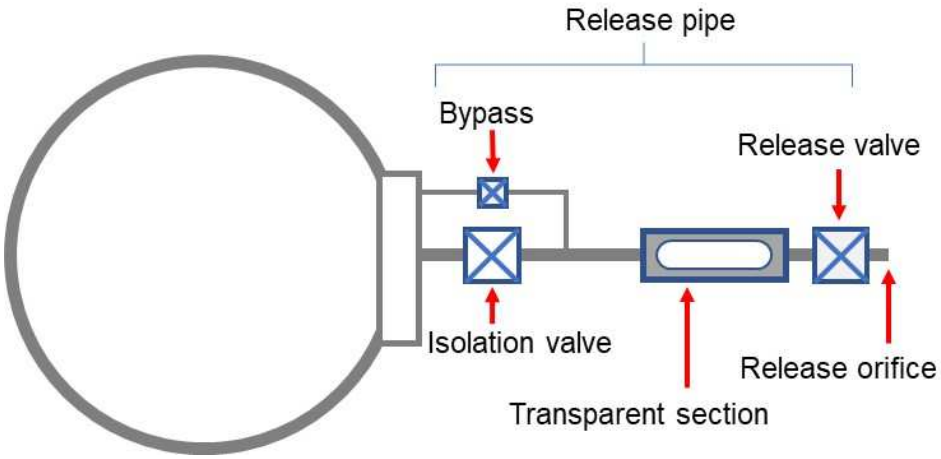

Figure 5: Schematic of the release pipe connected to the vessel with the valve setup

3. INSTRUMENTATION

A global view of the measurement systems is presented in Figure 6: about 8 thermocouples in the CO_2, 14 inside the wall of the vessel, 3 pressure gauges, 4 load cells (weight of the setup). More details about the range, accuracy and data management are given hereafter.

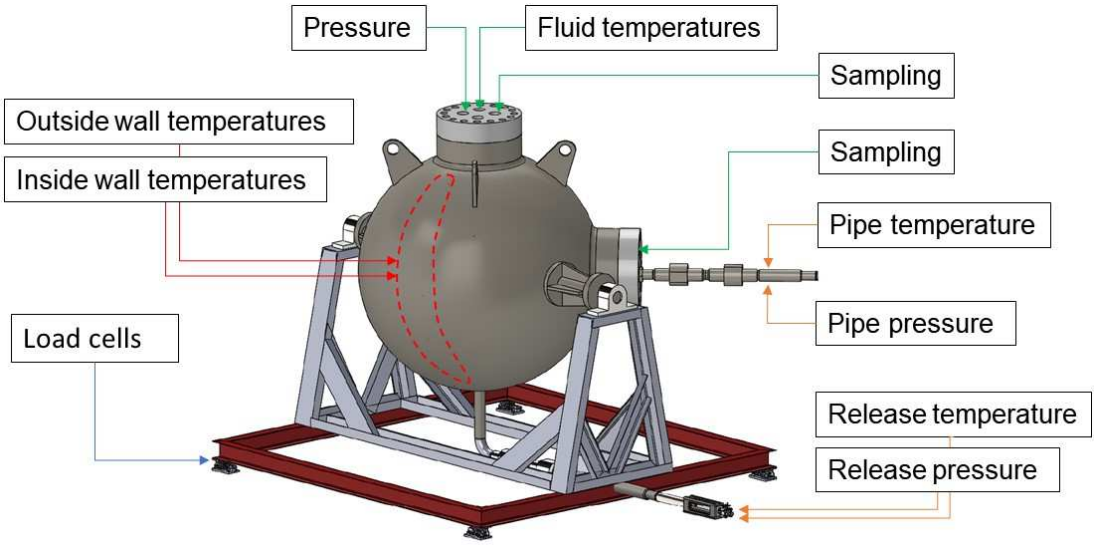

Figure 6: Drawing of the spherical vessel with instrumentation location

3.1 PRESSURE

Three pressure piezoresistive transducers are used to measure continuously the pressure inside the sphere, in the pipe, and immediately upstream of the release orifice. In the pipe, the pressure gauge is set in front of a thermocouple, giving the possibility to obtain local thermodynamic parameters such as density via a suitable equation of states.

Piezoresistive transducers are very efficient at measuring absolute pressures in static and dynamic conditions. Kistler 4043A type transducers, in the measuring range 0-200 bar, were used with an accuracy better than +/-0.2 bar. But they are

sensitive to temperature changes. Significant drift is expected outside the temperature range (-20°C to 50°C). As the temperature in the vessel may be as low as -50°C some thermal protection is required. To achieve this, they were mounted at the extremity of small pipes (8 mm inner diameter, 250 mm long), protruding outside the vessel insulation as shown in Figure 7.

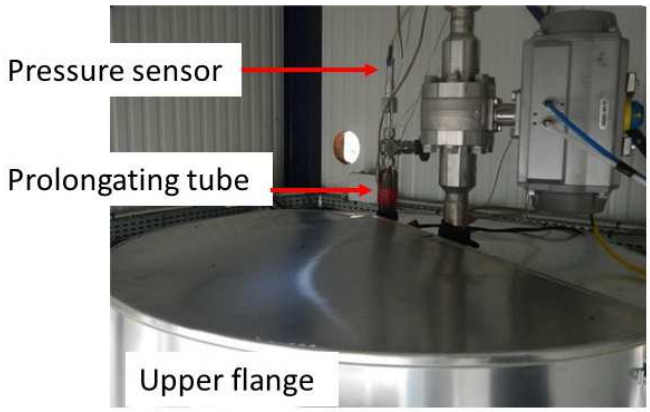

Figure 7: Pressure sensor connected to a prolongating tube installed on the upper flange

3.2 TEMPERATURE OF THE CO_2

The temperature of the CO_2 inside the vessel is measured at 6 locations along a vertical line using thermocouples (K type in stainless steel sleeve, 1.5 mm diameter, accuracy class 1 – absolute uncertainty: +/-1.5°C, step response time at 63%: less than 1 s). The thermocouples labelled Tc1 to Tc6 from the bottom to the top of the vessel, are attached on a vertical rod at the positions indicated in Figure 8.

Importantly, the supporting rod is graduated like a ruler (one graduation each 5 mm) so that it is possible to read directly the liquid level on the video.

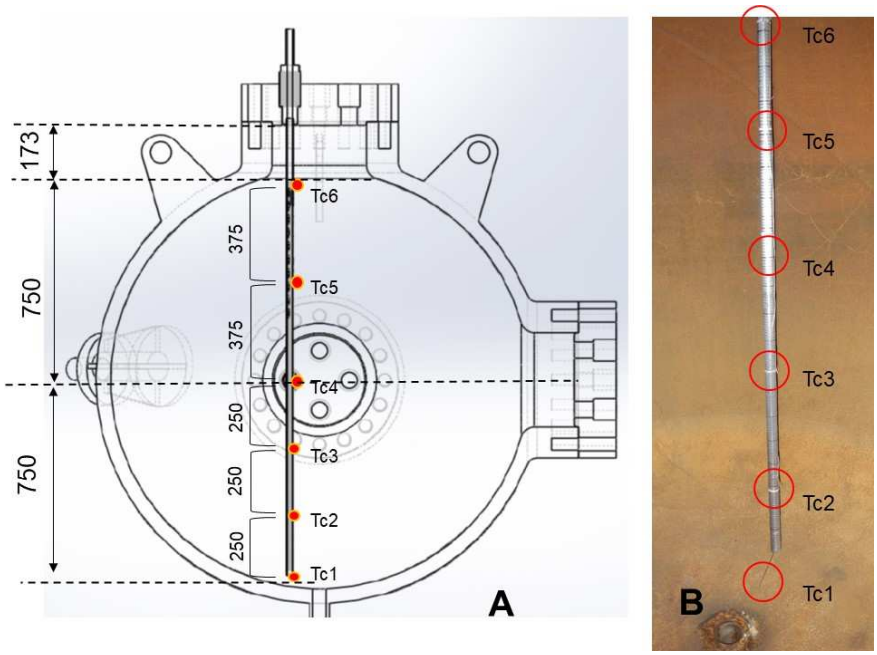

Figure 8 A: Location of the thermocouples inside the vessel. (A) Cross-sectional schematic of the vessel with the vertical rod supporting six K-type thermocouples (red circles). (B) Inside view of the vessel showing the rod with the thermocouple location

3.3 TEMPERATURE OF THE WALL

It was not possible to install temperature gauges on the inner wall of the vessel because of limited access. Thus, to estimate the temperature of the inner surface wall, it was decided to insert thermocouples (K type, bare wires, accuracy class 1 – absolute uncertainty: +/-1.5°C, step response time at 63%: less than 0.5 s) in 2 mm diameter holes drilled from the outside surface, ending at 5 mm from the inner surface. This way, the local (inner wall) temperature is obtained with limited thermal resistance. It was verified that these thermocouples follow the real-time inner surface temperature with a delay of about 1.5 s, which is short enough relative to the expected temperature changes inside the vessel during the expected blowdown period (hours).

The locations of the holes hosting the thermocouples are shown in Figure 9. The seven thermocouples are set approximately on the same meridian (opposite to the lateral flanges). These thermocouples are labelled Tci1 to Tci7 from the bottom to the top of the vessel. Thermocouple Tci6 is inserted slightly aside due to local obstructions.

The outside wall temperature is measured using seven more thermocouples attached to the outer surface of the vessel directly on the steel (K type, of the same design as inner wall thermocouples). They are located close to the holes where inner wall thermocouples are inserted.

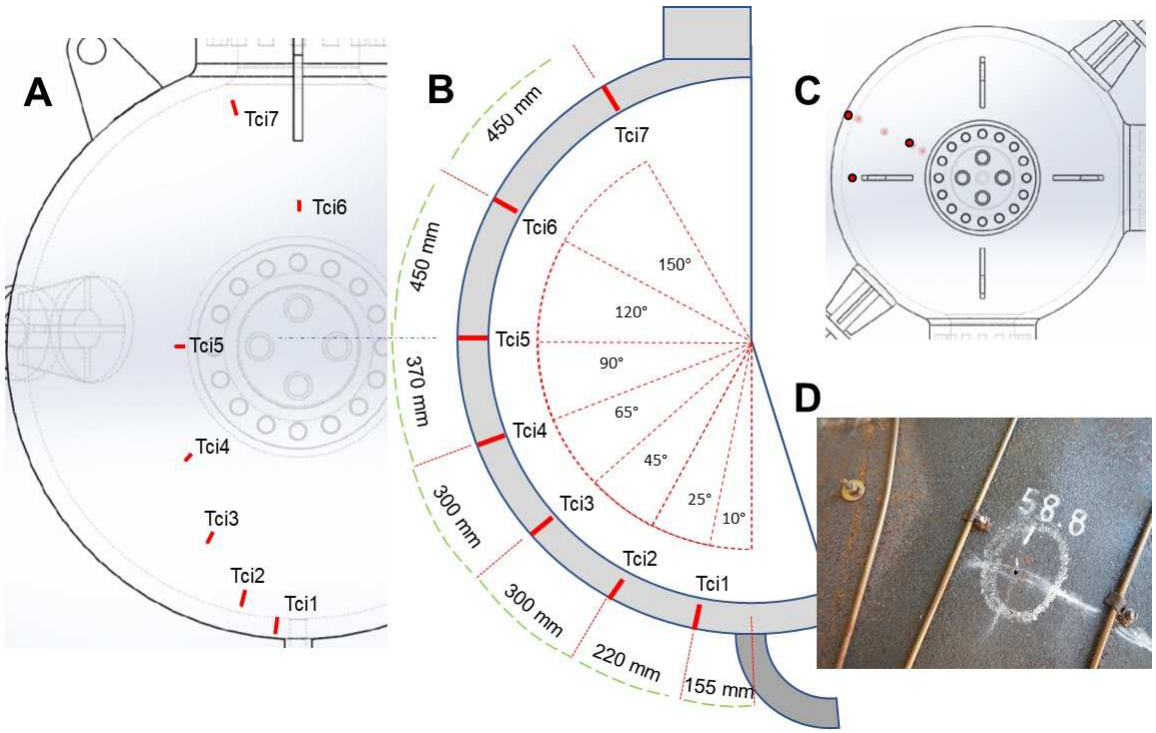

Figure 9: Schematics and picture of the vessel. (A) location of the seven holes drilled in the wall, (B) sectional view of the vessel indicating the exact location of the

holes in the vertical direction, (C) upper view showing the lateral offset of hole Tci6, (D) picture of one drilled hole with the local thickness of the vessel indicated

3.4 MASS FLOW RATE

The mass flow rate is an important parameter, for instance to close the heat balance. Several techniques were investigated. Intrusive techniques (Coriolis flowmeters, Venturi devices) were excluded to avoid any pressure loss (restriction, bends, split flow) in the release pipe. Non-intrusive techniques, namely ultrasonic probes, were tested both on liquid and gaseous releases. Due to the very strong acoustic absorption of gaseous CO_2 in a large pressure range (from 0.2 MPa to 1.5 MPa in the current configuration), unreliable results were obtained during gas releases. As bubbles strongly impair sound propagation, it proved impossible to monitor liquid releases with ultrasonic probes.

Because we faced those difficulties and since we tested this method with success in a previous study (CO2PipeHaz), it was decided to use scales to weigh continuously the vessel and derive the mass flowrate from the weight measurement. The vessel was installed on a strong steel square frame (see Figure 6) laid on 4 load cells (Mettler Toledo 0745A series, 2200 kg full scale each, ±100 g uncertainty). Since the supporting frame area is larger than the vessel imprint, the stability of the overall setup is guaranteed, reducing the oscillations that external wind or internal liquid movements may provoke. This issue was identified during previous test campaigns. A typical example is shown in Figure 10 A (blue curve) for the blowdown of the vessel occurring entirely in the gaseous domain (initial conditions: 50% CH_4, 50% CO_2, 10 MPa, 20 °C, 6 mm release diameter).

The evolution of the mass content M as a function of time t looks smooth, but a significant noise appears when deriving to obtain the mass flowrate (not shown). The raw data (M as a function of t) needs to be processed to reduce the signal-to-noise ratio. Since a monotonous mass loss is expected during a typical release, which lasts almost 30 minutes in this example, M should be a linear function of t over short enough periods typically several seconds in this example. Once such “short enough period of time” is defined - called in the following the “regression window” - a linear regression using the least square method is applied on each regression window to obtain the slope which gives the local mass flowrate. The regression window is moved over the total duration of the release to obtain the mass flowrate curve. This is the standard “running slope average” method which was implemented on standard spreadsheet.

Obviously, the accuracy of this method depends on the size of the regression window. The larger the size, the better the accuracy but the poorer the relevancy of the linear regression. An investigation of this aspect is presented below using the same example. It is possible to compute the “exact blowdown curve” (M-t) which is known to be an exponential decay during gaseous blowdown, since the mass flowrate is proportional to the pressure in the vessel (Weiss et al, 1988 for example). The best fit exponential decay law was derived from the experimental M-t curve and the derivation provided the “exact blowdown curve” named “model” in Figure 10. In Figure 10-A, the mass-time curve (blue line) is recorded at a sampling rate of 200 Hz and the mass flowrate calculation is performed over a regression window of 200 points meaning over 1 second (orange curve). The “exact” solution runs middle in the oscillations of the orange curve suggesting that the “running slope average method” applied to the raw data performs well. The uncertainty is the

deviation between the black and the orange curve. The “residuals” are calculated as the point-to-point difference between the running slope estimate and the exact solution. It is observed that the distribution of these residuals matches a centred normal law (Figure 10-B) suggesting there is no bias. The estimator of uncertainty is taken as the double of the standard deviation (σ) of the residuals (95% confidence interval) and is shown in Figure 10-C as a function of the size of the regression window (sample size).

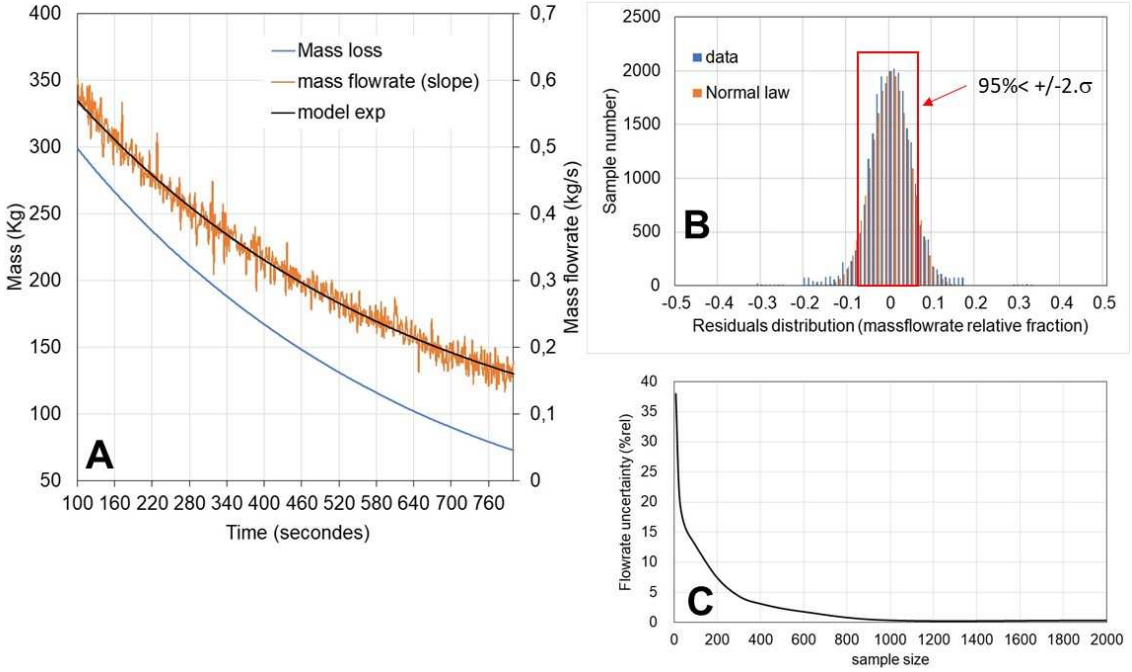

Figure 10: Effect of the size of regression window. (A) Example of a mass decrease recorded at a rate of 200 Hz (blue curve) and corresponding mass flowrate (orange curve) calculated with a running slope over 200 samples. The black curve is the exponential decay used as the exact blowdown curve, (B) Corresponding residuals distribution, (C) Flowrate uncertainty (± 2σ) as a function of the size of the regression window (or sample size)

It can be seen that the larger the sample size (i.e. the larger the duration of the “regression window”) the better the accuracy. Using more points offers the possibility to smooth out the vibrations of the vessel and the sources of noise. The upper limit would be the loss of linearly in the regression window. Here the larger regression window size is 2000 points meaning 10 seconds only which remains very small as compared to the characteristic time of the blowdown (about 600 seconds) for this specific case. In choosing the regression window size, attention should be paid to modification of the flow regimes like during phase changes. The size of the regression window should be as small as possible to detect such events.

Obviously, the sampling rate should not be larger than the cut-off frequency of the scales, otherwise, a different behaviour might appear (artificial data points are superposed on the real phenomena).

Experimentally this setup allowed to measure mass flowrate as small as 5 g/s provided that at least 400 g of CO_2 is released (the total uncertainty linked to a single mass measurement point). In principle, lower mass flowrate could be

measurable, but the result might be impaired by the potential drift of the load when the vessel would be submitted to a variation of external conditions (ambient pressure, wind) likely to happen over a long period of time.

3.5 LIQUID LEVEL AND VOLUME

The liquid level L_l can be measured as a function of time using the graduated vertical rod (Figure 11), with an uncertainty of +/- 2.5 mm. The volume of the liquid phase V_l can then be geometrically derived from:

$$V_l = \frac{\pi . {L_l}^2}{3} . (3R - L_l) \qquad [2]$$

the maximum uncertainty on V_l is +/- 4.5 l. This parameter is used to derive the apparent density of the liquid phase as shown later (§ 4.4).

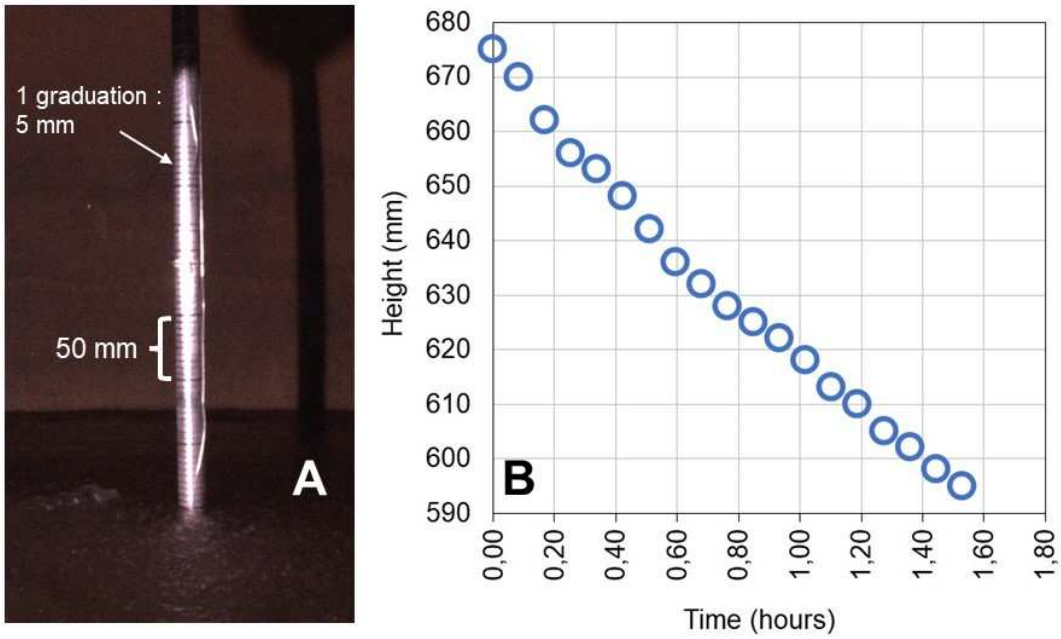

Figure 11: Liquid level in the vessel. (A) Detail of the graduated rod with marks every 5 mm. (B) Liquid level measured with time during the release

4. EXAMPLE OF RESULTS AND DISCUSSION

A typical test is run in two phases. In the first one, the vessel is filled with CO_2 in such a way that the desired initial conditions for the blowdown are reached as close as possible. As shown in section 4.1, this phase can be complicated and long. Then the blowdown phase is done. Results are presented in sections 4.2 to 4.4.

For the blowdown test phase chosen as an example (§4.2 to 4.4), 900 kg of pure CO_2 at 1 MPa and -38 °C were prepared and blown down from the middle flange (so in vapour regime), through an orifice of 4 mm. At the beginning of the release, the liquid surface is 10 cm below the axis of the release pipe.

4.1 COOLING OF THE VESSEL

Among other initial conditions, CO_2 blowdown experiments were carried out with low initial temperatures (down to -40 ºC). Several techniques were considered for cooling down the vessel to -40 °C. It appeared that the simpler and the faster was to make use of the refrigerant behaviour of CO_2 by vaporizing it directly inside the vessel. Thus, to do this a cryogenic storage vessel containing up to 3 tonnes of CO_2 was rented. The liquid CO_2 is stored at -25°C under 1.8 MPa and injected as a liquid inside the sphere where it evaporates totally at the beginning of the process and partially later. Since the pressure of the vessel increases during the cooling/filling process, CO_2 is vented periodically to maintain the pressure below that of the cryogenic vessel. Depressurization induces further CO_2 vaporization which drives the temperature further down.

Figure 12 gives an example of a cooling/filling operation. At time t=700 s, thermocouples Tc1 and Tc2 are submerged in 480 kg of liquid at -38 °C. Several gas discharges (three, between t=700s and t=1100 s) decrease the pressure. The liquid temperature drops to -50 °C (due to vaporization), while about 50 kg of CO_2 is flushed out. From time t=2600 s to 2900 s, 200 kg of liquid CO_2 is injected, which slightly increases the liquid surface temperature (Tc2). Part of this injected CO_2 vaporizes and increases the pressure. During CO_2 injection, the gas phase temperatures first decrease, and then equilibrate due to the mixing effect of the CO_2 jet. When the pressures between the storage container and the vessel equilibrate (at t=2900 s), the CO_2 injection stops. Depressurization/filling operations are repeated at time t=3000 s and t=3300 s allowing introduction of 250 kg CO_2 while flushing out about 40 kg.

The whole process allowed the introduction of 400 kg of CO_2 in the vessel, mostly liquid, and the decrease of liquid temperature down to -45 °C. During the process, 90 kg of CO_2 evaporated, extracting about 30 MJ, mainly from the liquid phase and from the bottom of the sphere, sharpening the thermal gradient in the fluid and along the wall of the vessel. Cooling of the liquid (the mass initially present in the vessel and the quantity introduced) required about 11 MJ. The difference (30 - 11=19 MJ) corresponds to the heat extracted from the steel (4 tonnes, 450 kJ/kg/K, meaning a temperature decrease of 10 °C).

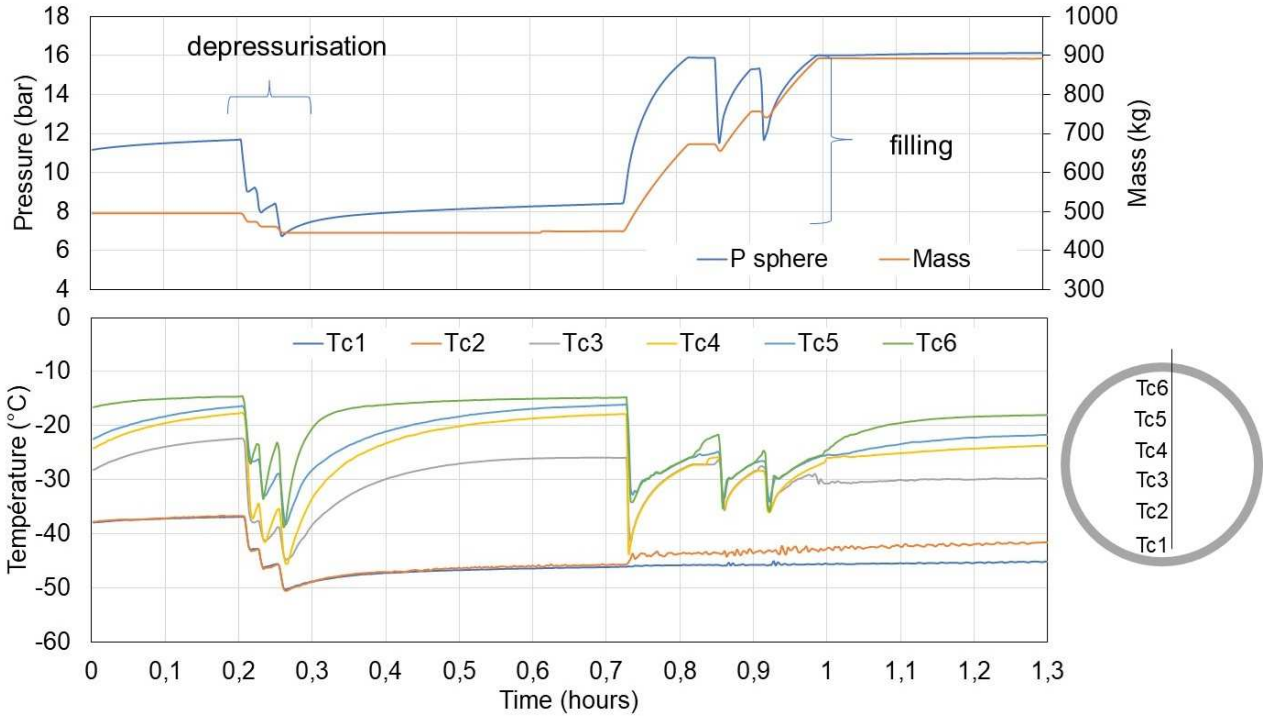

Figure 12: Example of a depressurization/filling process and the impact on fluid temperature

After the cooling/filling process is finished, sufficient time is allowed for the vessel to reach the test conditions and reach a steady state. For instance, about 60 hours were required (Figure 13) to reach -15 °C starting from a situation very similar to the one illustrated in Figure 12. Note that a vertical temperature gradient remains between the liquid and the gas phase even after 3 days suggesting a very stable and stratified vapour phase and the absence of convection currents.

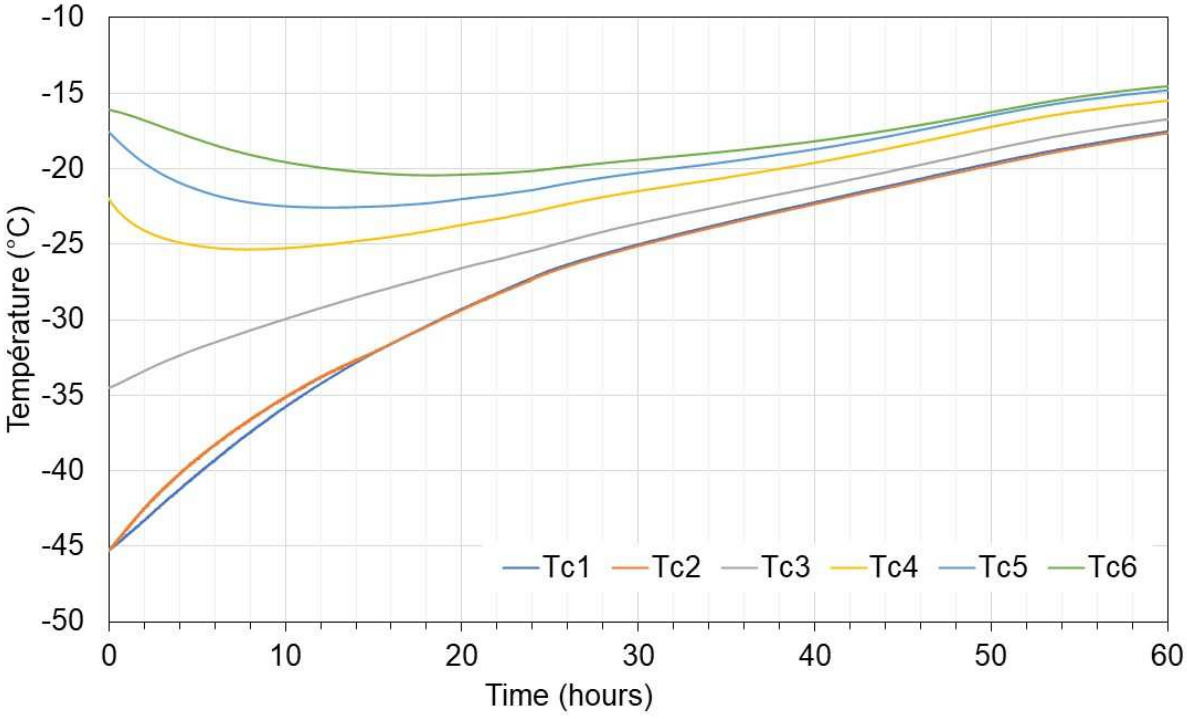

435 Figure 13: Fluid temperature evolution after a filling operation similar to the one
436 illustrated in Figure 12. Initial time starts when filling is completed
437

438 ## 4.2 PRESSURE AND MASS FLOWRATE

439 Pressure and mass flowrate as a function of time are presented in Figure 14. A
440 video of the interior of the vessel was done and excerpts are inserted in Figure 14.
441 A vapor-solid-liquid system is observed when the pressure reaches the triple point
442 of CO_2 (0.5185 MPa and -56.6 °C according to NIST database). Once the remnant
443 liquid phase has evaporated, after a plateau of more than 4 hours (Figure 14 A),
444 only dry ice remains and the pressure drops since the evaporation rate of the solid
445 is smaller than that of the liquid (as seen in the mass flowrate curve, Figure 14 B).
446 One piece of explanation could be that the sublimation heat is much larger than the
447 vaporization heat (543 kJ/kg vs 347 kJ/kg) but another one that disappearance of
448 the convective heat transfer when liquid has evaporated leaves only heat
449 conduction at work, which is a slow process. The total duration of this blowdown
450 operation is very long, more than 15 hours. Although the blowdown was not finished
451 the flowrate was so small that the recordings were stopped.

452 The pressures in the vessel, in the pipe and just upstream of the orifice are almost
453 equal (Figure 14 A): indicating that head losses are small under the present test
454 conditions. The volumetric flowrate in the pipe calculated from the mass flowrate,
455 the pressure and the gas temperature is indeed very low: about 1.5 l/s at its
456 maximum, meaning a gas velocity in the pipe of at most 1 m/s. This is too low to
457 generate measurable pressure losses.

458 To interpret the pressure-time curve shown in Figure 15 (solid line), the saturated
459 vapour pressure at the thermodynamic equilibrium was calculated based on the
460 measured liquid temperature Tc3 (note that the temperature is homogenous in the
461 liquid phase as shown in the next subsection) and vapour liquid equilibrium
462 equation from NIST database. The corresponding theoretical curve is superposed
463 as a dotted line. The two curves seem close to each other. It is difficult to interpret
464 accurately the discernable slight deviations because of the uncertainties of the
465 measurements.
466

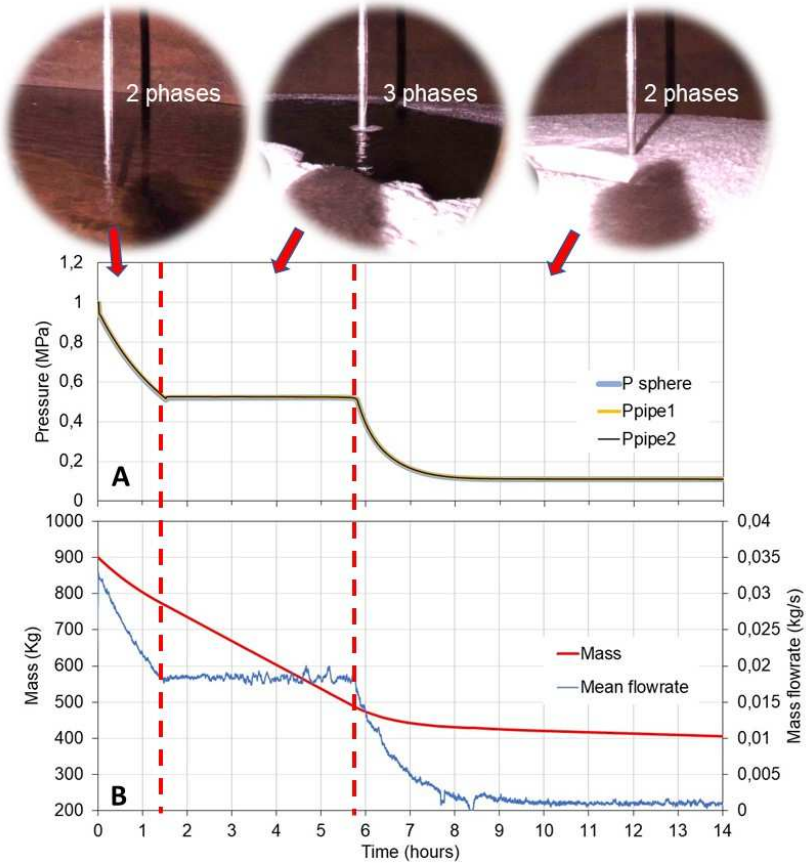

Figure 14: pressure (A) and mass/ mass flowrate (B) recorded during the release. The pictures extracted from the video illustrate the three stages observed.

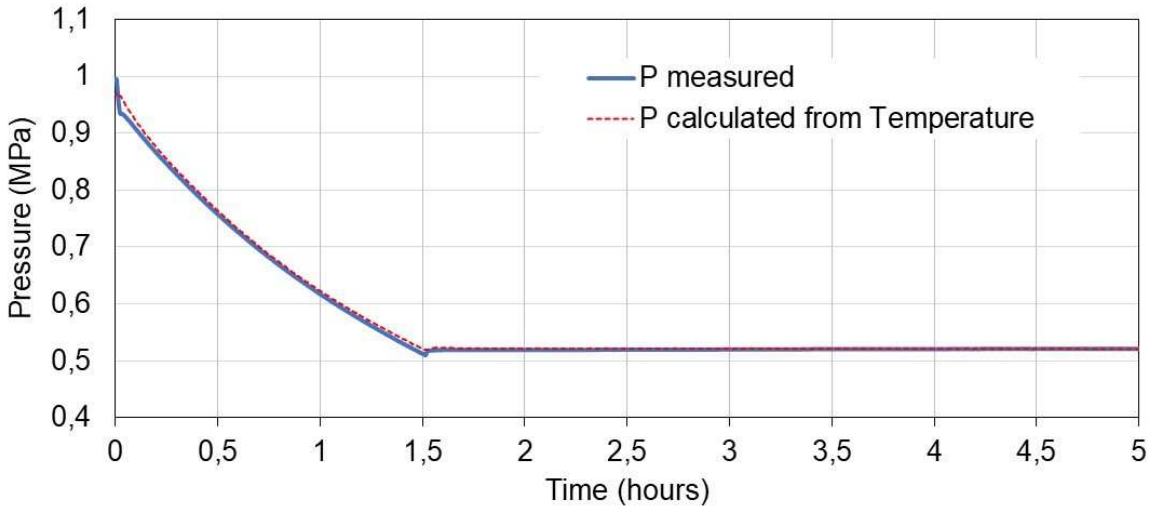

Figure 15: Excerpts of the pressure profile, zooming on the beginning of the release (A) and on the period when dry ice appears (B).

4.3 HEAT TRANSFER

Figure 16 shows the evolution of the temperatures measured inside the vessel in the CO_2 fluid (Figure 16-A) and along the wall at 5 mm from the inner face of the vessel (Figure 16-B).

The temperature within the dense CO_2 phase remains homogeneous, whether in its liquid or solid state. However, the temperature gradient in the gas phase, which is initially significant (10 °C at t = 0 s), intensifies during the release due to the decreasing temperature of the gas/liquid (or gas/solid) interface. Consequently, the vapour expelled at the interface between the dense phase and vapour becomes increasingly cold, while the temperature of the upper part of the gaseous phase remains relatively unchanged, suggesting a restricted heat transfer and stratification within the vapor phase. In contrast, in the condensed phase, the heat transfer rate should certainly be much larger ensuring the homogeneity of the temperature field. Evaporation of CO_2 requires a large quantity of energy which is expected to be mostly extracted from the liquid phase but possibly also from the steel shell in contact with the liquid, and from the vapour via the vapour-liquid interface. This could explain why, as observed, a large temperature gradient is created between the upper part and the bottom part (Figure 16) inside the shell of the vessel. A tentative estimate of these various heat fluxes is proposed hereafter.

The thermal flux through the shell along the circumference *reads*:

$$\phi = (\lambda_{st}/_{C}).A.(T_{up} - T_{bo}) \qquad [3]$$

where A, the cross-section of the shell at mid-height of the vessel is 0.3 m^2, (T_{up}-T_{bo})= 20 °C and C the characteristic length of the temperature gradient. In the present context the order of magnitude of C is R. Then, the thermal flux through the shell is about Φ= 330W.

About the thermal exchanges between the vapour phase, the vessel wall on the sides and the liquid interface at the bottom, it should be first observed that, since the hot area is at the top of the vessel, a stratified stable mixture is obtained in the gas phase. In such conditions, Huetz (Huetz et al, 1990) demonstrated that heat exchange is mostly due to thermal conduction. As shown on Figure 16 during the vaporization phase, the temperatures measured at the same elevation in the vapour phase (Tc4, Tc5 and Tc6) and in the shell (Tci5, Tci6 and Tci7) are the same within the accuracy range implying a very small amount of heat exchange between the vapour phase and vessel wall. Considering now the thermal exchange with the liquid interface, expression [3] can be used again taking A as the area of the liquid interface (approximately the cross section of the vessel: A=1.9 m^2), C again close to R and the average temperature difference of 10°C. The thermal conductivity of the vapour is 0.016 W.m/K so that the thermal flux between the vapour phase is only 0.8W. As a result, the evolution of the gas mixture is nearly adiabatic during the blowdown so that the stratification increases.

It is then clear that heat is nearly exclusively extracted from the liquid phase a temperature drop at the bottom of the vessel is induced, producing the observed temperature gradient along the meridians of the vessel shell.

The characteristics of the heat exchanges between the liquid phase and the outside can also be analyzed. Since the pressure is constant during the vaporization phase, the leakage flowrate (CO_2 leaving the vessel at a rate of 19 g/s between time 1.5 h

and 6 h after the beginning of the release: Figure 13) is compensated by the evaporation rate. The liquid-vapour latent heat of vaporization is 370 kJ/kg (NIST database), meaning a required power of 7000 W to sustain the evaporation. This is much larger than the thermal flux through the shell of the vessel (330W) and through the liquid interface (0.8 W) so that nearly all the vaporization power is extracted from the liquid phase itself. This a nearly adiabatic process (not more than 5% of the required heat comes from outside the liquid phase).

The last point is about the phase changes inside the liquid. During the vaporization, the pressure and temperature (0.52 MPa, -56.6 °C) correspond to the triple point conditions, and dry ice is also produced (Figure 14) to deliver this flux (the latent heat of solidification is 200 kJ/kg). The heat of vaporization is certainly extracted from the bulk of the dense phase via nucleate boiling and multisite crystallization so that the heat exchange rate is large enough for the temperature in the dense phase to be homogenous. However, when the liquid has disappeared (typically after t=8h on Figure 16), this equilibrium is lost. The reason could be that the thermal exchanges are weak in the solid structure of dry ice.

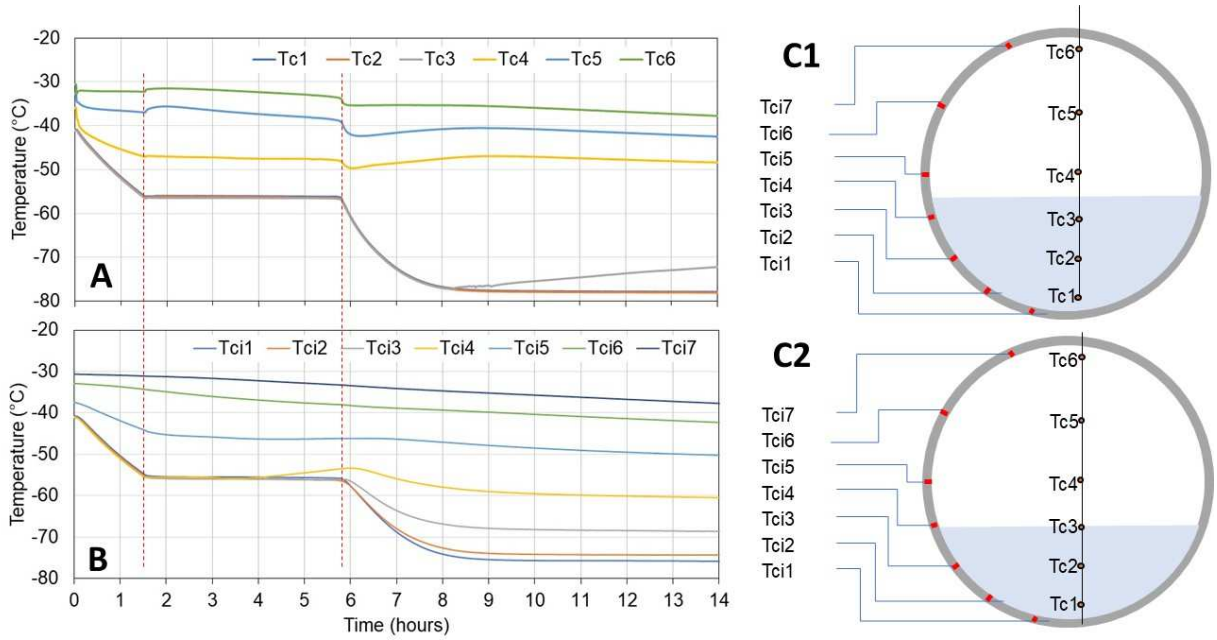

Figure 16: Temperature profile of the fluid. (A) inside the vessel (Tcx) and (B) in the inner wall surface (Tcix) during the release. On the right side, drawings of the vessel showing (C1) the location of the gas/liquid interface at t= 0 (C1) and (C2) the location of the gas/solid interface at the end of the test (t= 14 h)

4.4 DENSE PHASE DENSITY

At the opening of the release valve (Figure 15), the dense phase is liquid and the pressure-temperature trajectory, as described in section 4.2, follows the trend of the vapor-liquid equilibrium. As explained in section 3.5, the liquid level L_l can be

550 measured as a function of time using the graduated vertical rod (Figure 11), and the
551 volume of the liquid phase V_l can be derived from [2].
552 The mass of liquid can be obtained from the measured total mass of CO_2 m_{fl},
553 knowing the vapour mass:
554 $$m_l = m_{fl} - (V_{fl} - V_l).\rho_g \qquad [4]$$
555
556 The density of the vapor ρ_g is calculated from the pressure and temperature in the
557 gas phase and the volume of the fluid $V_{fl}$is equal to the internal volume of the
558 vessel. The apparent density of the liquid $\rho_l = {}^{m_l}/_{V_l}$ can then be obtained.
559 The combined uncertainties of liquid level, mass, pressure and temperature lead to
560 +/-1.5 %, with a major effect of the liquid level uncertainty. The calculation of the
561 vapour density may be affected by the bias attached to the temperature of the gas
562 phase, which is obtained from averaging Tc4, Tc5 and Tc6 values. However, it has
563 been verified that an error of 5°C propagated in the calculation of the liquid density
564 has an impact lower than 0.1%.
565
566 The results are presented in Figure 17-A (liquid density versus temperature) and
567 Figure 17-B (liquid density versus pressure) together with the uncertainty margin.
568 On the same graphs the standard value of the liquid density ρ is shown (NIST
569 Database; equation of state: Span, Wagner (1996)). Clearly the experimental values
570 (open points) are below the standard theoretical value (solid line). It is believed that
571 this difference is due to the presence of vapour bubbles inside the evaporating
572 liquid (the homogeneity of the temperature in the liquid suggests a sort of nucleate
573 boiling which might be forced by the high release rate). The fraction of volume *Vl*
574 occupied by vapour bubbles can then be estimated as:
575 $$VF_g = \frac{(\rho_l - \rho_{fl})}{\rho_l} \qquad [5]$$
576 Over the total duration of this release, an average value of 1.4% for VF_g is
577 calculated.
578

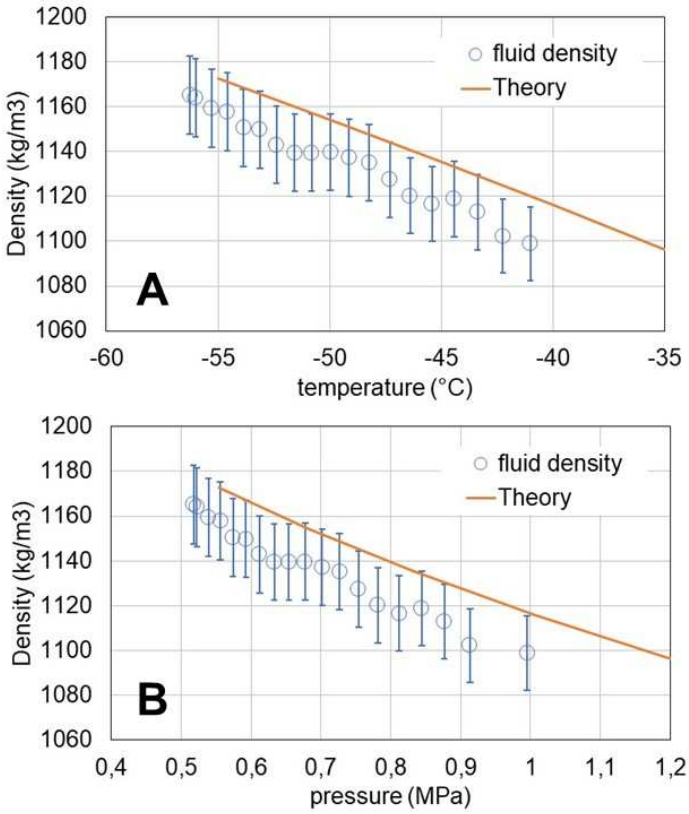

Figure 17 A: Liquid density versus temperature. B: Liquid density versus pressure. Error margin corresponds to an uncertainty of +/-1.5%

Once dry ice appears the dense phase level remains almost steady for several hours (Figure 18). The density of the solid CO_2 is larger than that of the liquid (NIST database) but the blocks of solid are floating, suggesting a foam-like structure with bubbles of vapour inside. An expert eye may recognize this structure in Figure 19. It completely covers the surface in about 20 minutes while the liquid phase slowly disappears (in about 4 hours) at the bottom of the vessel.

Within the present test conditions, where the only vapour phase was vented out, visual inspection through the transparent section shows that no mist, droplets or dry ice particles were circulating in the release pipe.

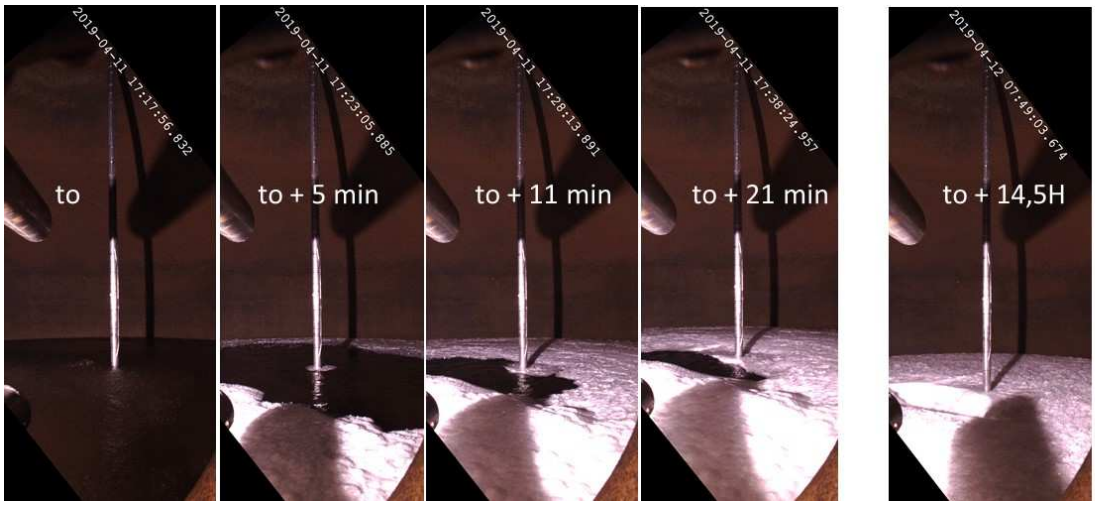

Figure 18: images of the fluid showing dry ice formation as a function of time.

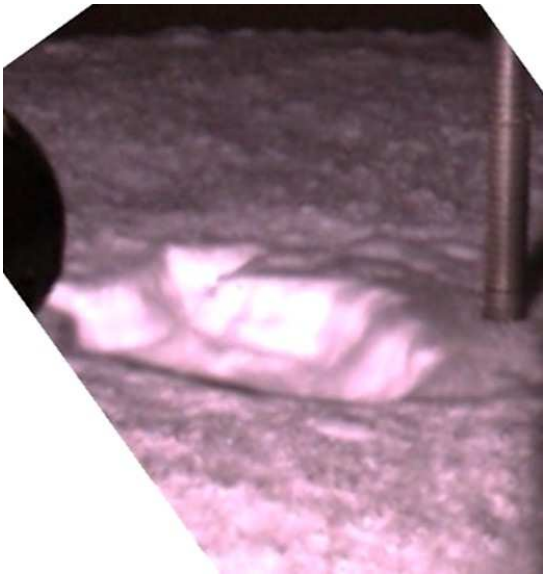

Figure 19: Close-up showing the dry ice foam-like structure. Image extracted from a video taken several hours after complete vaporization of the liquid phase

5. CONCLUSIONS

The context is the safety of transfer operations of CO_2 within the frame of CCS deployment. Operators fear that the large temperature drop following the release may lead to the rupture of equipment and that dry ice plugs block and damage the transfer lines as already observed. Because three phases may coexist and because various heat transfer regimes may intervene, the modelling task is difficult and experimental data are required to map such scenarios. The objective of the present work is to prepare and qualify an experimental device to produce the missing experimental data.

To this purpose, a specific experimental setup was designed to investigate in detail the blowdown of a vessel containing CO_2. The instrumentation of the device was chosen to enable an accurate monitoring of pressure, temperature, phase transitions and mass flowrate during the blowdown.

The vessel is a 2 m^3 sphere, thermally insulated and connected to a release pipe 40 mm inner diameter (2 m long) fitted with a discharge orifice to control the depressurization rate. The vessel is carefully insulated. The measurement techniques include:

- the pressure (3 points) and the temperature of the CO_2 inside the vessel (6 points along the vertical axis) and in the release pipe (2 points),
- the temperature inside the thickness of the wall of the sphere (7 points along a meridian),
- the continuous weighting of the vessel content.

Optic ports were installed to monitor the liquid level and observe phase transitions in the vessel (and in the pipe).

The way to monitor the mass flowrate is discussed in some detail. The experimental device (sphere, pipe, valves, …) is supported by 4 electronic scales providing an estimate of the total mass within ±0.4 kg for a total mass of 4 tonnes. But using an adequate data regression technique called the “running slope average” method the mass flowrate uncertainty is found to be as low as ±5%. The method proved efficient both for gaseous and liquid releases for flowrates ranging from kilograms per second to a few grams per second. This is an important aspect not only in the purpose of controlling the experimental conditions but also in view of providing a robust technique to calibrate the flow metering devices to be installed on the transport network.

A typical blowdown case is presented starting from 900 kg of liquid CO_2 stored in the vessel under 1 MPa and -38°C releases through a 4 mm orifice (vapour phase releases). The triple point is reached during the blowdown and the coexistence of the three phases was captured in the video recordings. The dry ice appears as a sort of island floating on the liquid CO_2 which continues to vaporize and crystallize. During this process the pressure and the temperature of the dense phase are constant. The sublimation phase starts after complete solidification and the release mass flowrate drops significantly. The residence time seems very long, much more than 10 hours.

Before reaching the triple point, an expected two-phase vaporization is observed with a gradual cooling of the liquid accompanied by a drop of the pressure. The density of the liquid is below that of the pure liquid suggesting the presence of bubbles of vapour inside the liquid and some form of bulk nucleation. Most of the heat exchanges seem to occur inside the CO_2, into the dense phase, where the heat of vaporization and sublimation is extracted probably via bulk nucleation and crystallization. Heat exchanges between the vapour phase and the liquid surface and the wall of the vessel are very small leading to a highly stratified vapour phase. Although of a limited extent (as compared to what happen inside the CO_2 dense phase), heat exchanges between the vessel and the CO_2 take place between the liquid CO_2 and the wall. They are strong enough to cool the bottom part of the vessel to the lowest temperature of the dense phase, about -75°C.

As discussed in the present paper, the dimensions of the device are chosen to be representative of real situations in terms of size effects (volume, thickness,..). Thermal conditions obtained are also mimicking for instance cryogenic storage. A pure cryogenic CO_2 blowdown test is presented but further experiments are intended to cover other conditions including tests with CO_2-containing impurities.

.

Acknowledgment

This work was performed within the frame of a Joint Industry Project (JIP) called CARDICE (for CARbon Dioxide ICE). This JIP was set-up by TotalEnergies, Equinor, Ineris and Petrell. It was partly supported by Gassnova under CLIMIT-Demo project.

REFERENCES

Bjelić M. B., Kovanda K., Kolařík L., Vukićević M. N., Radičević B. S. (2015). Numerical modeling of two-dimensional heat-transfer and temperature-based calibration using simulated annealing optimization method: application to gas metal arc welding. Thermal Science, 2016, vol. 20, no. 2, pp. 655-665

Chaineaux J. (1993). MERGE Project, final report. E.U. DG XII contract.

Chaineaux J. (1995). EMERGE Project, final report. INERIS Contribution.

CLIMIT Demo project CARDICE – https://climit.no/en/project/cardice - last access 07/02/2023

CO_2PipeHaz - Quantitative Failure Consequence Hazard Assessment for Next Generation CO_2 Pipelines: The Missing Link. 2009. http://www.co2pipehaz.eu/

European Zero Emission Technology and Innovation Platform (ZEP) (2021). A Trans European CO_2 Transportation Infrastructure for CCUS – Opportunities – Challenges. https://zeroemissionsplatform.eu.

France Nord (2012). Des aquifères salins pour stocker le CO_2. ADEME https://www.ademe.fr/france-nord.

Gant S.E.; Narasimhamurthy V.D.; Skjold T.; Jamois D.; Proust C. (2014). Evaluation of multi-phase atmospheric dispersion models for application to Carbon Capture and Storage. Journal of Loss Prevention in the Process Industries, 32 286-298.

Haque M. A., Richardson S. M., Saville G. (1992). Blowdown of pressure vessels I. Computer model. Trans IChemE, Part B, Proc Safe Env Prot, 70(B1) 3-9.

Haque M. A., Richardson S. M., Saville G., Chamberlain G., Shirvill L. (1992). Blowdown of pressure vessels II. Experimental validation of Computer model and Case studies. Trans IChemE, Part B, Proc Safe Env Prot, 70(B1) 10-17.

Huetz J., Petit J.P. (1990). Notions de transfert thermique par convection. Les techniques de l'ingénieur A 1 540.

Jamois D., Proust C., Hebrard J., Gentilhomme O. (2013). La sécurité du captage et du stockage du CO_2: un défi pour les industries de l'énergie. XIV^e Congrès de la Société Française de Génie des Procédés (SFGP), Lyon, France, 8-10 October 2013. Récents Progrès en Génie des Procédés, Numéro 104 – 2013, ISSN: 1775-335X; ISBN: 978-2-910239-78-7, Ed. SFGP, Paris, France, 2013.

Jamois D., Proust C., Hebrard J. (2015). Hardware and instrumentation to investigate massive spills of dense phase CO_2. Canadian Journal of Chemical Engineering, 93 (2) 234-240.

Lacome J.M.; Lemofack C.; Jamois D.; Reveillon J.; Duret B.; Demoulin F.X. (2020). Experimental data and numerical modeling of flashing jets of pressure liquefied gases. Process Safety Progress, art. prs12151.

Martynov S., Zheng W., Mahgerefteh H., Brown S., Hebrard J., Jamois D., Proust C. (2018). Computational and Experimental Study of Solid-Phase Formation during the Decompression of High-Pressure CO_2 Pipelines. Industrial and Engineering Chemistry Research, 20 7054-7063.

NIST Database – http://www.nist.gov/

Peletiri S. P., Rahmanian N., Mujtaba I. M. (2018). CO_2 Pipeline Design: a review. Energies, 11, 2184.

Span, R., Wagner, W. (1996). A New Equation of State for Carbon Dioxide Covering the Fluid Region from the Triple-Point Temperature to 1100 K at Pressures up to 800 MPa. J. Phys. Chem. Ref. Data **1996**, 25, 1509– 1596

Talemia R. H., Brown S., Martynov S., Mahgerefteh H. (2016). Hybrid fluid-structure interaction modelling of dynamic brittle fracture in pipeline steel transporting CO_2 steams. International Journal of Greenhouse Gas Control, 54, 702-715.

Weiss M.H., Botros K.K., Jungowski W.M. (1988) Simple Method Predicts Gas Line Blowdown Times, Oil & Gas Journal, Dec. 12, 1988

Witlox H.; Harper M.; Oke A.; Bowen P. J.; Kay P.; Jamois D.; Proust C. (2009). Two-phase jet releases and droplet dispersion: scaled and large-scale experiments, droplet-size correlation development and model validation. Hazards Symposium - Manchester, UK - Hazards XXI: Process Safety and Environmental Protection in a Changing World - 615-623.

Woolley R.M., Fairweather M., Wareing C.J., Falle S.A.E.G., Proust C., Hebrard J., Jamois D. (2013). Experimental measurement and Reynolds-averaged Navier-Stokes modelling of the near-field structure of multi-phase CO_2 jet releases. Int. J. Greenhouse Gas Control, 18 139-149.

Woolley R. M.; Fairweather M.; Wareing C.J.; Falle S. A. E. G.; Mahgerefteh H.; Martynov S.; Brown S.; Narasimhamurthy V.D.; Storvik I.; Saelen L.; Skjold T.; Economou I. G.; Tsangaris D. M.; Boulougouris G. C.; Diamantonis N.I.; Cusco L.; Wardman M.; Gant S. E.; Wilday J.; Zhang Y.C.; Chen S.; Proust C.; Hebrard J.; Jamois D. (2014). CO_2PipeHaz: quantitative hazard assessment for next generation CO_2 pipelines. Energy Procedia, 63: 2510-2529 - International Conference on Greenhouse Gas Technologies (GHGT-12), 05/10/2014 - 09/10/2014, Austin, US.

Zheng W., Mahgerefteh H., Jamois D., Hebrard J., Proust C. (2017). Modeling of depressurization-induced superheating for compressed liquefied gases. Industrial & Engineering Chemistry Research, 2017, 56 (18): 5432-5442.